JACS
JOURNAL OF THE AMERICAN CHEMICAL SOCIETY

Article

pubs.acs.org/JACS

Simultaneous Time-Dependent Surface-Enhanced Raman Spectroscopy, Metabolomics, and Proteomics Reveal Cancer Cell Death Mechanisms Associated with Gold Nanorod Photothermal Therapy

Moustafa R. K. Ali,[§,‡] Yue Wu,[§,‡] Tiegang Han,[§] Xiaoling Zang,[§] Haopeng Xiao,[§] Yan Tang,[⊥] Ronghu Wu,[*,§] Facundo M. Fernández,[*,§] and Mostafa A. El-Sayed[*,§,#]

[§]School of Chemistry and Biochemistry, Georgia Institute of Technology, Atlanta, Georgia 30332-0400, United States
[⊥]School of Biology, Georgia Institute of Technology, Atlanta, Georgia 30332, United States
[#]School of Chemistry, King Abdul Aziz University, Jeddah 21589, Saudi Arabia

Supporting Information

ABSTRACT: In cancer plasmonic photothermal therapy (PPTT), plasmonic nanoparticles are used to convert light into localized heat, leading to cancer cell death. Among plasmonic nanoparticles, gold nanorods (AuNRs) with specific dimensions enabling them to absorb near-infrared laser light have been widely used. The detailed mechanism of PPTT therapy, however, still remains poorly understood. Typically, surface-enhanced Raman spectroscopy (SERS) has been used to detect time-dependent changes in the intensity of the vibration frequencies of molecules that appear or disappear during different cellular processes. A complete proven assignment of the molecular identity of these vibrations and their biological importance has not yet been accomplished. Mass spectrometry (MS) is a powerful technique that is able to accurately identify molecules in chemical mixtures by observing their m/z values and fragmentation patterns. Here, we complemented the study of changes in SERS spectra with MS-based metabolomics and proteomics to identify the chemical species responsible for the observed changes in SERS band intensities during PPTT. We observed an increase in intensity of the bands at around 1000, 1207, and 1580 cm^{-1}, which were assigned in the literature to phenylalanine, albeit with dispute. Our metabolomics results showed increased levels of phenylalanine, its derivatives, and phenylalanine-containing peptides, providing evidence for more confidence in the SERS peak assignments. To better understand the mechanism of phenylalanine increase upon PPTT, we combined metabolomics and proteomics results through network analysis, which proved that phenylalanine metabolism was perturbed. Furthermore, several apoptosis pathways were activated via key proteins (e.g., HADHA and ACAT1), consistent with the proposed role of altered phenylalanine metabolism in inducing apoptosis. Our study shows that the integration of the SERS with MS-based metabolomics and proteomics can assist the assignment of signals in SERS spectra and further characterize the related molecular mechanisms of the cellular processes involved in PPTT.

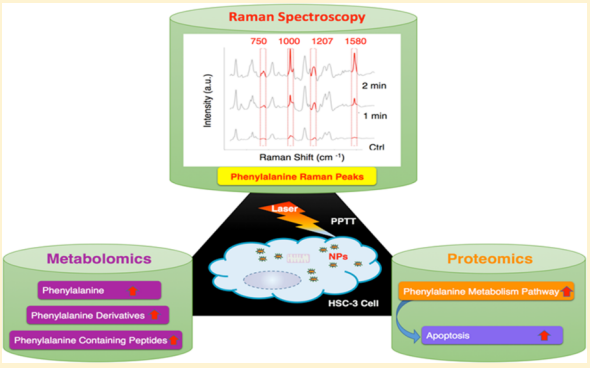

INTRODUCTION

Plasmonic nanoparticles offer a powerful means to follow dynamic changes associated with intracellular molecular events in real time.[1−3] Their localized surface plasmon resonance (LSPR) confers these particles unique optical properties. For example, the electromagnetic fields on the surface of plasmonic nanoparticles are greatly increased and exhibit exponential decay patterns following non-radiative (heat) or radiative (e.g., light-scattering) processes.[4,5] Raman scattering from the molecules localized near the plasmonic nanoparticles' surface is therefore enhanced by orders of magnitude, resulting in the well-known surface-enhanced resonance spectroscopy (SERS) phenomenon.[6,7] SERS has been successfully applied to single-cell analysis, where plasmonic gold nanoparticles are placed inside the cell and the resulting SERS spectrum collected in order to record the intracellular microenvironment changes occurring over time near the nanoparticles. Our group reported on the spectral changes observed by SERS during the full cell cycle of a single cancer cell. The time required to kill cancer cells, associated with the time taken for the SERS spectrum to stop changing when the cells were given anti-cancer drugs[4,8] or were heated,[9] was also determined. However, the molecular species associated with the observed SERS bands could not be

Received: August 22, 2016
Published: November 3, 2016

DOI: 10.1021/jacs.6b08787
J. Am. Chem. Soc. 2016, 138, 15434−15442

confidently assigned, preventing elucidation of the molecular mechanisms involved in these critical cellular processes.

Photothermal therapy has its foundation in the targeted destruction of cancerous cells via the heat released by gold nanorods (AuNRs) following near-infrared (NIR) radiation absorption. The so-called "water wavelength window" between 700 and 1200 nm is widely considered to be the optimal spectral region for conducting PPTT,[10,11] as tissue and water absorption are minimized in this range. AuNRs, on the other hand, readily absorb NIR laser light, resulting in effective photothermal generators for both *in vitro* and *in vivo* applications. AuNRs-based PPTT has been successful at inducing cancer cell apoptosis,[12] resulting in *in vivo* tumor removal.[13−16]

Despite the operational success of PPTT, the molecular mechanisms associated with PPTT-induced apoptosis remain largely unknown or under dispute. We observed PPTT-induced apoptosis initiated through heat-shock proteins previously,[17] while several reports indicate it is mediated by the mitochondrial apoptotic pathway via Bid activation and caspase 3 activity.[18,19] Although SERS reports on the real-time biomolecular dynamics in the microenvironment associated with the PPTT process, SERS spectra from cells are incredibly complex, reflecting overlapping signals from a variety of proteins and metabolites that are difficult to assign to individual species. It has been reported, for example, that the 1000 and 1580 cm^{-1} peaks showed significant increases during cell apoptosis,[8,20] with great debate about their assignment.[21] One report in the published literature assigned the 1000 cm^{-1} signal to phenylalanine,[22] while a different report assigned it to tryptophan.[21] Furthermore, it has been argued[8] that these SERS signals actually reflect changes in protein structure, a topic that is still being intensively debated. One hypothesis states that the 1000 cm^{-1} signal is indicative of the exposure of protein hydrophobic rings following conformational changes,[8] while others report that the protein conformation change induced by adding methanol or sodium dodecyl sulfate (SDS)[23] or increasing temperature[9] does not alter the intensity of the 1000 cm^{-1} peak, contradicting the hypothesis that this signal is associated with alterations in protein conformation.

Herein, we monitored the SERS spectral signature *in vitro* during apoptosis as a function of PPTT exposure time. We also performed metabolomics and proteomic studies on cell lysates under identical PPTT conditions. Integrative multi-omics network analysis revealed specific alterations that explain the underlying changes in SERS spectral data, demonstrating the power of combining SERS with MS for studying cellular processes following PPTT.

RESULTS

Formulation of AuNRs and Cell Uptake. To perform PPTT inside human oral squamous cell carcinoma (HSC-3) cells, AuNRs were used in order to efficiently convert NIR light into heat. The AuNRs were synthesized using a seedless method[24] (see Supporting Information (SI) for experimental details) with an average size of 25 nm × 6 nm, as shown in Figure 1b (transmission electron microscopy (TEM) image), and an absorption maximum at about 800 nm (as shown in the UV−vis spectrum in Figure 1c). This particle size is favorable in conducting PPTT, as it has better efficiency for conversion of light into heat.[25]

For formulation of AuNRs@NLS, we first used methoxy-polyethylene glycol thiol (mPEG-SH) to modify the surface of

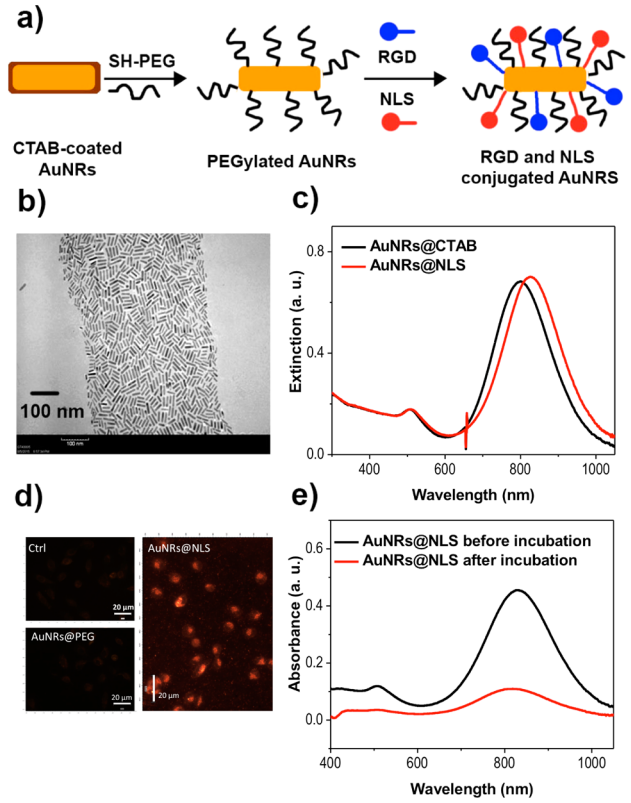

Figure 1. Characterization of conjugated AuNRs and measurement of HSC-3 (human squamous carcinoma) cell endocytosis with AuNRs. (a) Schematic showing the surface conjugation of the AuNRs with PEG, followed by RGD and NLS. (b) Transmission electron microscopy (TEM) image of conjugated AuNRs. Scale bar = 100 nm. (c) UV−vis absorption spectra of the unconjugated AuNRs (black spectrum) and AuNRs conjugated with NLS (red spectrum). (d) Dark-field images of control HSC-3 cells (not exposed to AuNRs), cells exposed to AuNRs@PEG, and cells exposed to AuNRs@NLS for 24 h. Scale bar = 20 μm. (e) UV−vis absorption spectra of the AuNRs@NLS dispersed in culture media before (black spectrum) and after (red spectrum) incubation with cells.

AuNRs to gain better biocompatibility.[26] The PEGylated particles were then functionalized with Arg-Gly-Asp (RGD) peptides (known to bind to Rvβ6 integrin on the surface of cancer cells to enhance the receptor-mediated endocytosis of the nanoparticles[27]) and nuclear localization signal (NLS) peptides (peptide sequences that are recognized by importin and translocate near the nucleus[28]), as shown in Figure 1a. Successful surface modification of AuNRs@NLS is evident in the red-shift of the plasmon peak of AuNRs, from 800 nm for the as-synthesized AuNRs to 825 nm for AuNRs@NLS (Figure 1c). The zeta potentials of the AuNRs at different stages were measured (SI, Table S1) to confirm surface modifications. The as-synthesized cetyltrimethylammonium bromide (CTAB)-coated AuNRs had highly positive surface charges, as imparted by the CTAB cationic surfactant. Following PEG modification, the AuNRs became negatively charged (−10.2 ± 6.73 mV). The zeta potential of the AuNRs became positive again after further modification of the RGD and the NLS peptides.

The uptake of AuNRs was first monitored by dark-field (DF) microscopy. The HSC cells were incubated with a 2.5 nM concentration of AuNRs for 24 h. For AuNRs@NLS, as shown in the DF image (Figure 1d), clear internalization was observed compared with cells not exposed to AuNRs and cells exposed

DOI: 10.1021/jacs.6b08787
J. Am. Chem. Soc. 2016, 138, 15434−15442

to AuNRs without targeting agents. The DF image shows that AuNRs@NLS accumulated in nuclear regions. In addition, the UV−vis spectra of culture media with AuNRs before and after incubation with cells were also collected (Figure 1e), which showed a decrease of the peak intensity that reflects the portion of AuNRs being uptaken by the cells. Differential interference contrast (DIC) microscopy also confirmed the cellular internalization of AuNRs@NLS (SI, Figure S1). In summary, AuNRs were successfully formulated and then introduced into cells with good cell uptake. The cell viability and apoptosis were tested under different concentrations of AuNRs. The results indicate that the concentration of the AuNRs utilized in this study is much lower than that affecting cell viability or inducing apoptosis (SI, Figure S2).

SERS of Cancer Cells Undergoing AuNRs-Based Photothermal Therapy. The AuNRs with dimensions 25 nm × 6 nm[24] and concentration 2.5 nM were selected for use for heat generation. After incubation with AuNRs for 24 h, a continuous-wave (CW) 808 nm NIR laser with power of 5.8 W/cm^2 [25,29,30] was used for irradiation of the cells for different time intervals. The laser wavelength overlapped with the longitudinal SPR peaks of the AuNRs. The temperature rose to 45 °C after 2 min of laser exposure. The effect of PPTT was confirmed using a cell viability assay and an apoptosis/necrosis assay. The cell viability results showed a significant decrease in the percentage of viability (~40%) for the HSC cells incubated with AuNRs (2.5 nM) after exposure to the 808 nm NIR laser for 3 min (SI, Figure S3). In the apoptosis/necrosis assay, cells were labeled with Annexin V and propidium iodide (PI), and the fluorescent signals were examined by flow cytometry. As shown in SI, Figure S3, the number of apoptotic cells significantly increased after PPTT was applied. The decrease of cell viability and increase of apoptosis indicated the efficacy of PPTT.

For real-time SERS measurement, spectra were collected at a single spot of cells to avoid variations due to changing location. A 785 nm laser was focused on a single cell, and spectra were recorded. As our AuNRs have weak SERS signals (due to their small size), in order to enhance the signals, 40 nm gold nanospheres (AuNSs) with the same surface modification as AuNRs were used to assist the detection.[27] Detailed information about AuNSs@NLS characterization and cellular uptake is given in SI, Figure S4. The introduction of AuNSs does not affect AuNRs uptake or SERS spectra shapes during the PPTT process due to their small amount and the fact that they do not absorb NIR light (SI, Figures S5 and S6a). SERS spectra of HSC cells without PPTT were comparable with our previous publications;[8,31,32] possible assignments for each peak are given in SI, Table S2. Upon NIR laser exposure, the band around 1000 cm^{-1} increased in intensity, due mainly to the benzene ring breathing of phenylalanine as mentioned before.[33] Though in most publications this band is assigned to phenylalanine, some debate is still going on regarding its assignment.[23,34] Further, we observed that the enhancement of the 1000 cm^{-1} peak was accompanied by the enhancement of the 1207 and 1580 cm^{-1} bands (Figure 2a), which are attributed to the in-plane CH stretching vibration and side-chain vibration coupled with the in-phase motion corresponding to phenylalanine.[8,35,36] The same experiment was repeated three times, and the same trend of peak intensity changes of 1000, 1207, and 1580 cm^{-1} was obtained (Figure 2b and SI, Figure S7). SERS of cells 12 h after PPTT has also been performed to confirm that the signal remains altered (SI, Figure S8). On the other hand, a control experiment was conducted on cells without laser exposure. No obvious SERS spectral change was observed during NIR laser irradiation of the control (SI, Figure S6b). This gave us more evidence of the phenylalanine increase after the PPTT process.

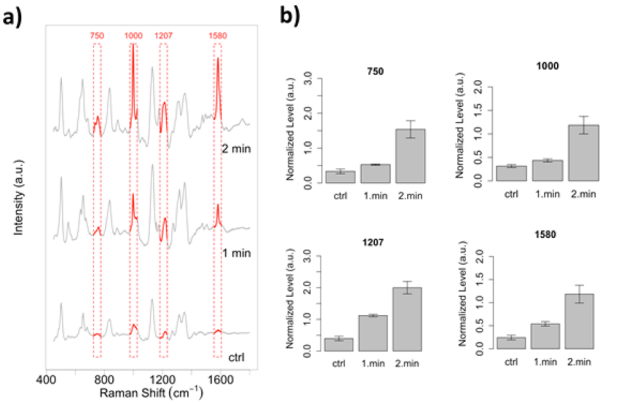

Figure 2. (a) SERS spectra collected from a single HSC-3 cell under NIR laser exposure (808 nm diode laser, 5.8 W/cm^2) at 1 and 2 min delays. The 750, 1000, 1207, and 1580 cm^{-1} bands are shown in red and placed in red boxes. (b) Bar graphs of the Raman bands associated with biomolecules located within the AuNP plasmonic field.

Generally, we can rule out the possibility of tryptophan contributing to the 1000 cm^{-1} signal since side-chain vibrations in its SERS spectrum appear at 758, 869, 1011, 1357, 1410, 1546, and 1602 cm^{-1}, corresponding to the counterparts at 756, 874, 1009, 1358, 1423,1558, and 1619 cm^{-1} in the solid Raman spectrum.[37] However, our SERS data did not show obvious increases of these peaks. Therefore, our SERS results support the conclusion that the phenylalanine increases in the microenvironment around the nanoparticles during PPTT.

In addition to the phenylalanine bands, we also observed a 750 cm^{-1} band whose intensity increases during PPTT (Figure 2), which has been assigned to the pyrrole breathing mode ν_{15} in cytochrome *c*.[38,39] This result suggested the increase of apoptotic cells during thermal heating through cytochrome *c*-mediated apoptosis. This result is in agreement with our flow cytometry data (SI, Figure S3), indicating that PPTT triggered apoptosis.

Metabolomics and Proteomics Experiments Confirming Perturbation of Phenylalanine Metabolism during AuNRs PPTT. For metabolomics experiments, we analyzed the metabolites of cells using liquid chromatography−mass spectrometry (LC-MS). Two biological replicates and two technical replicates were conducted. A total of 1122 tentative features (retention time (t_R), m/z pairs) were detected in metabolite extracts, corresponding to 152 metabolites with detectable ($[M - H]^-$) primary ion. Hierarchical clustering analysis on the similarity matrix of metabolomics data was carried out to verify the reproducibility of the experiments (SI, Figure S9b). Among these, 238 metabolomics features were differentially expressed in the AuNR@NLS-treated group when compared to the control group (FDR = 0.05, corresponding to p = 0.015) (SI, Figure S9e); 483 metabolomics features were differentially expressed in the AuNR@NLS/PPTT group when compared to the control group (FDR = 0.05, corresponding to p = 0.015) (SI, Figure S9f). Specifically, many of these features corresponded to an increase in the relative amount of phenylalanine (Figure 3a) and related species after PPTT (Figure 3b−d and SI, Figure S10). Phenylalanine derivatives

DOI: 10.1021/jacs.6b08787
J. Am. Chem. Soc. 2016, 138, 15434−15442

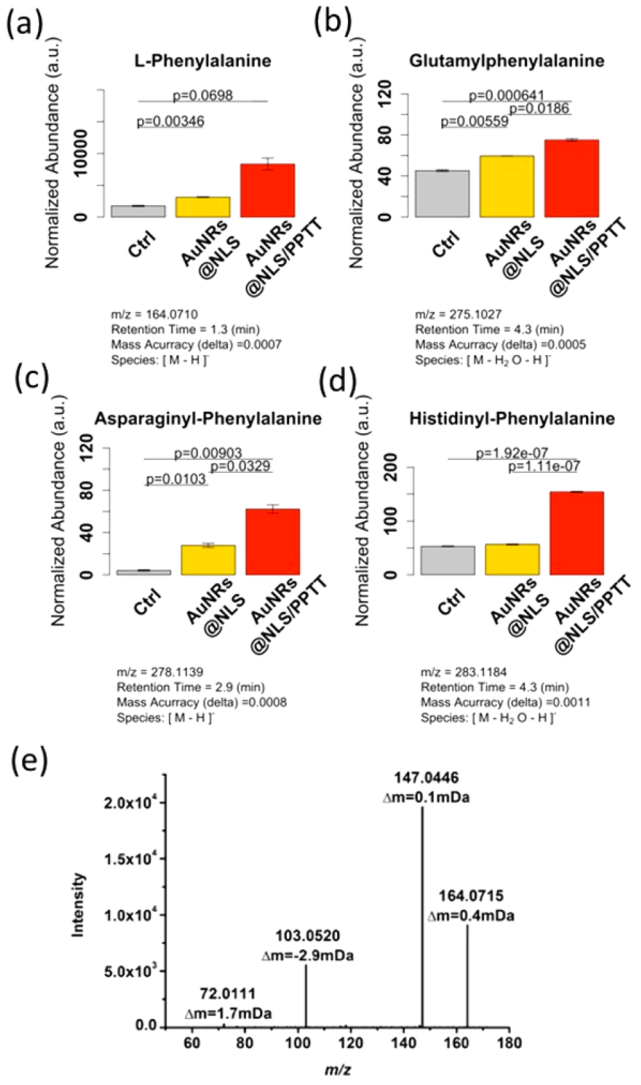

Figure 3. Metabolite perturbations observed in HSC-3 cells treated with AuNRs-PPTT (NLS conjugated particles). (a–d) Bar graphs showing the normalized abundance of phenylalanine-related metabolites altered following PPTT: (a) L-phenylalanine (the result was confirmed by MS/MS, shown in panel e); (b) glutamyl-phenylalanine; (c) asparaginyl-phenylalanine; and (d) histidinyl-phenylalanine. Normalized abundances of metabolites following AuNRs@NLS without PPTT are also given for comparison. (e) Product ion spectrum obtained under data-dependent acquisition conditions for the precursor ion at m/z 164.0710. Matching of this mass spectrum to the Metlin database MS/MS reference spectrum of phenylalanine (10 V collision energy) is shown, with mass accuracies indicated for each ionic species detected.

and phenylalanine-containing short peptides, such as glutamyl-phenylalanine (Figure 3b), asparaginyl-phenylalanine (Figure 3c), and histidinyl-phenylalanine (Figure 3d), were among those altered, explaining the trends observed in the SERS data. Tandem MS experiments confirmed the identity of the species detected by MS with excellent accuracy (Figure 3e).

Furthermore, we also conducted a label-free quantitative proteomics experiment for studying alterations in protein abundances and seeking possible evidence for, and understanding of the mechanisms responsible for the phenylalanine concentration increase. A test experiment was done to measure the accuracy of our proteomics workflow using the reported method,[66] where 99% of the proteins have shown accurate quantification (SI, Figure S11). In our proteomics experiment, two biological replicates and three technical replicates were conducted. Clustering analysis (SI, Figure S9a) indicated good reproducibility for the proteomics experiments. In total, 1341 proteins were identified. Among these, 326 proteins were differentially expressed in the AuNR@NLS-treated group compared to the control group (SI, Figure S9c); 278 proteins were differentially expressed in the AuNR@NLS/PPTT-treated group in contrast to the control group (SI, Figure S9d).

Proteomics results were integrated with metabolomics for a more holistic understanding of the biological processes involved. Integrated pathway analysis showed that the phenylalanine metabolism pathway was significantly perturbed by PPTT (SI, Figures S12 and S13). Approximately half of the metabolites in the phenylalanine metabolism pathway were identified as changed, including 2-phenylacetamide (increase), phenylpyruvate (decrease), 2-hydroxy-3-phenylacrylic acid (decrease), 3-oxobutanoate (increase), fumarate (increase), phenylacetaldehyde (increase), L-tyrosine (decrease), 4-fumarylacetoacetate (decrease), and 4-maleylacetoacetate (decrease). These alterations were accompanied by perturbations in several key proteins in the phenylalanine metabolism pathway.

Elevated levels of phenylalanine are known to induce apoptosis,[36,37] which is consistent with the apoptotic phenotype observed in PPTT-treated cells. An overview of pathways identified as being related to phenylalanine-induced apoptosis is schematically shown in Figure 4a. Two proteins in the phenylalanine metabolism pathway have been previously

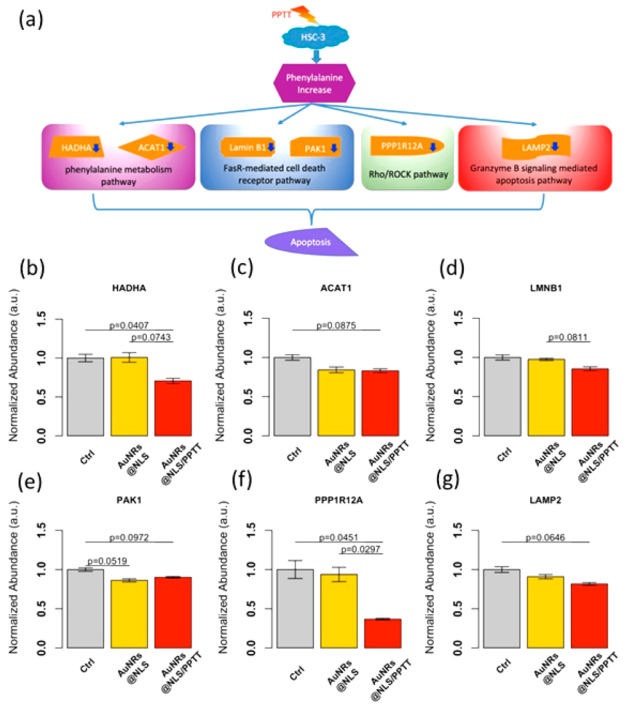

Figure 4. (a) Schematic diagram explaining the molecular apoptosis mechanisms involved in altering phenylalanine metabolism as induced by PPTT. (b–g) Bar graphs showing the normalized abundance of key proteins contributing to apoptosis involved in altering phenylalanine metabolism following PPTT: (b) HADHA, (c) ACAT1, (d) Lamin B1 (LMNB1), (e) PAK1, (f) PPP1R12A, and (g) LAMP2. Normalized abundances of key proteins following AuNRs@NLS without PPTT are also given for comparison.

DOI: 10.1021/jacs.6b08787
J. Am. Chem. Soc. 2016, 138, 15434–15442

associated with apoptosis. Mitochondrial acetyl-CoA acetyltransferase (ACAT1) has been shown to be involved in the development of doxorubicin resistance to decrease cell apoptosis.[42] Another mitochondrial protein, hydroxyl-coenzyme A dehydrogenase/3-ketoacyl-coenzyme A thiolase/enoyl-coenzyme (HADHA), has been shown to prevent chemically induced apoptosis in cancer treatment.[43,44] In our experiments, both proteins were observed to be down-regulated following PPTT treatment, suggesting that the anti-apoptotic protection was turned off resulting in enhanced vulnerability to apoptosis (Figure 4b,c).

In addition to the phenylalanine metabolism pathway, three possible mechanisms of phenylalanine-induced apoptosis were suggested by the results. First, increased phenylalanine was shown to induce apoptosis by involvement of the Fas receptor (FasR)-mediated cell death receptor pathway.[41] In this study, two proteins (Lamin B1 and PAK1) in the Fas/Fas ligand death receptor pathway were identified. These two proteins have been previously demonstrated to be associated with apoptosis. Lamin B1, as the major component of the nuclear lamina underlying the nuclear membrane, plays an important role in maintaining nuclear membrane integrity. Destruction of nuclear membrane integrity being a hallmark of apoptosis. During apoptosis, Lamin B1 mRNA level have been shown to decrease,[45] which could result from induction of either p53 or pRB tumor suppressor pathways.[46,47] Literature results also show that the Fas/Fas ligand complex downstream effector PAK1 is required to prevent apoptosis by limiting the expression of pro-apoptotic proteins or modulating post-translational modifications on effectors.[48−50] In this study, both of these proteins were down-regulated, suggesting a cellular shift toward apoptosis, and reduced anti-apoptotic protection (Figure 4d,e).

Phenylalanine has also been shown to activate mitochondria-mediated apoptosis through the Rho/ROCK pathway.[40,51] In this study, we identified down-regulation of the myosin phosphatase targeting subunit 1 (PPP1R12A) in PPTT-treated cells, this being a downstream effector of ROCK (Figure 4f) that would contribute to the apoptotic phenotype following PPTT. In apoptotic cells, PPP1R12A is cleaved, with the cleaved PPP1R12A inhibiting myosin II binding, which results in membrane blebbing and apoptosis.[52,53]

A third mechanism of phenylalanine-induced cell death involves a component in Granzyme B signaling-mediated apoptosis, known as lysosome-associated membrane protein 2 (LAMP2). This protein was down-regulated following PPTT treatment (Figure 4g). LAMP2 is critical to maintain lysosome integrity and normal cellular function, and lower levels of LAMP proteins have been positively associated with apoptosis.[49] It is not yet conclusively established, however, whether decreased LAMP2 levels are also directly associated with phenylalanine-induced apoptosis.

DISCUSSION

Time-dependent SERS has recently enabled researchers to probe molecular changes in single (cancer) cells over time during the full cell cycle, or as the cell dies from exposure to drugs or from heat treatment. SERS accurately follows changes in cellular and subcellular environments during the onset and progression of processes such as apoptosis and mitosis[8,32] in real time and at a single-cell level. Cells present several active molecular Raman bands associated with biomolecules located within the AuNP plasmonic field.

Herein, we coupled SERS measurements with metabolomics and proteomics experiments performed on the same set of samples, aiming to study the change of the subcellular microenvironment around AuNRs during the PPTT process. Our SERS data showed that the 1000, 1207, and 1580 cm^{-1} bands increased during PPTT, which suggested an increase of phenylalanine and its derivatives. These findings were confirmed with whole cell metabolomics experiments using high-resolution mass spectrometry. We observed an increase of free phenylalanine, together with an increase of its derivatives and phenylalanine-containing peptides. Integrative analysis of proteomics and metabolomics data also showed that the proteins and metabolites in the phenylalanine metabolism pathway related to apoptosis were perturbed in apoptosis direction. Elevated levels of phenylalanine have been implicated in mitochondria-mediated apoptosis through Rho/ROCK pathway and Fas/Fas ligand mediated apoptosis.[40,41,51] In this study, both pathways were changed in favor of apoptosis in PPTT, where the level of phenylalanine was increased. In addition, the results suggested that, during phenylalanine-induced apoptosis, lysosome integrity may have been perturbed, which may further contribute to cell death. This hypothesis was further strengthened by the observation of an increasing pattern of pyrrole breathing mode ν_{15} in cytochrome *c* shown in the SERS spectra (750 cm^{-1}), which suggests the increase of apoptotic cells during thermal heating through cytochrome *c*-mediated apoptosis, which is in agreement with flow cytometry data (SI, Figure S3). Meanwhile, some other apoptosis pathways were revealed by proteomics, shown in SI, Figure S14.

Further investigations into the mechanism of how PPTT treatment increases phenylalanine levels in cells focused on the fact that phenylalanine can be converted to L-tyrosine.[54−56] Metabolomics data indicated that, after PPTT treatment, the level of L-tyrosine was actually decreased (SI, Figure S12). Based on our results, the channel allowing for the conversion from phenylalanine to L-tyrosine could have contributed to the accumulation of phenylalanine, which further induced mitochondria-mediated apoptosis.

We observed in our results (Figures 3, 4, and S10) that several metabolites/proteins change abundance in the presence of AuNRs even without light exposure, possibly due to the gold nanoparticles alone which could perturb apoptosis pathways of the biological system, as has been reported previously.[57,58] This effect, however, compared to the effect of PPTT treatment on apoptosis pathways, occurs to a much smaller extent and did not cause actual apoptosis (SI, Figure S2).

Besides the phenylalanine-dependent process, we further identified significantly perturbed pathways by integrative analysis of proteomics and metabolomics (SI, Figure S13). Other amino acid metabolism pathways are enriched, including methionine-cysteine-glutamate and lysine metabolism, both of which are very essential for the basic survival of the cells. Interestingly, we also found clues on the perturbation of pathways related to lipid metabolism and ketone body metabolism.[59−61]

In conclusion, by integrative analysis of Raman spectroscopy profiles, metabolomics, and proteomics mass spectrometric data, we discovered that free phenylalanine and associated metabolites are significantly perturbed by PPTT, leading to cell apoptosis. We therefore propose that phenylalanine measurements by SERS can be developed as a sensitive and convenient readout for non-invasive direct apoptosis characterization.

DOI: 10.1021/jacs.6b08787
J. Am. Chem. Soc. 2016, 138, 15434−15442

EXPERIMENTAL SECTION

Materials. Tetrachloroauric acid trihydrate ($HAuCl_4 \cdot 3H_2O$), trisodium citrate, $NaBH_4$, ascorbic acid, CTAB, $AgNO_3$, 4-(2-hydroxyethyl)-1-piperazineethanesulfonic acid (HEPES), NaCl, and sodium deoxycholate (SDC) were purchased from Sigma-Aldrich (USA). Methoxypolyethylene glycol) thiol (mPEG-SH, MW 5000) was purchased from Laysan Bio, Inc. Cell-penetrating peptide RGD (RGDRGDRGDRGDPGC) and nuclear localization signal NLS (CGGGPKKKRKVGG) peptides were obtained from GenScript, Inc. Dulbecco's phosphate-buffered saline (PBS), Dulbecco's modified Eagle's medium (DMEM), fetal bovine serum (FBS), antibiotic solution, and 0.25% trypsin/2.2 mM EDTA solution were purchased from VWR. Mammalian cell protease inhibitors were purchased from Roche Applied Sciences, sequencing grade trypsin was purchased from Promega, and Lysyl endopeptidase (Lys-C) was from Wako.

Instrumentation. Gold nanoparticles were imaged using a JEOL 100CX-2 transmission electron microscope, and their average size was then measured by ImageJ software. UV−vis spectra were obtained using an Ocean Optics HR4000CG UV−NIR spectrometer. SERS spectra were collected using a Renishaw InVia Raman microscope equipped with a 785 nm diode Raman excitation laser and a Leica optical microscope. Comprehensive metabolomics analyses were performed with ultra-performance liquid chromatography−mass spectrometry (UPLC-MS), using a Waters ACQUITY UPLC H Class system fitted with a Waters ACQUITY UPLC BEH C18 column (2.1 mm × 50 mm, 1.7 μm particle size, Waters Corp., Milford, MA, USA), coupled to a Xevo G2 QTOF mass spectrometer (Waters Corp., Manchester, UK) with an electrospray ionization source. The typical resolving power and mass accuracy of the Xevo G2 QTOF mass spectrometer were 25 000 (fwhm) and 1.8 ppm at m/z 554.2615, respectively. Proteomics analysis was done on a hybrid dual-cell quadrupole linear ion trap−orbitrap mass spectrometer (LTQ Orbitrap Elite, Thermo Fisher) with Xcalibur 3.0.63 software. Flow cytometry experiments were conducted on a BD LSR II flow cytometer (BD Biosciences).

Synthesis, Conjugation, and Characterization of AuNSs and AuNRs. Gold nanospheres with an average diameter of 30−40 nm were synthesized using the citrate reduction method.[62] Briefly, 200 mL of 0.254 mM $HAuCl_4 \cdot 3H_2O$ solution was heated until boiling and then reduced by adding 5 mL of 0.35% of trisodium citrate. The solution was then left heating until it turned wine red, followed by cooling under water flow. The citrate-stabilized AuNSs were first centrifuged at 5000g for 10 min and then redispersed in deionized (DI) water to remove extra citrate for the next step of conjugation. AuNRs with an average size of 25 nm × 6 nm (length × width) were synthesized using a seedless growth method.[24] Briefly, 5 mL of 1.0 mM $HAuCl_4$ was added to a mixture of 5 mL of 0.20 M CTAB, 250 μL of 4.0 mM $AgNO_3$, and 8 μL of 37% HCl. Next, 70 μL of 78.8 mM ascorbic acid was added, and then 15 μL of 0.01 M of ice-cold $NaBH_4$ was immediate injected. The solution was left undisturbed for 12 h, followed by centrifugation at 21000g for 50 min. It was redispersed in DI water, and a second centrifugation at 19000g for 40 min removed the extra CTAB. TEM was used to measure the sizes and homogeneity of the nanoparticles. AuNSs and AuNRs were then conjugated according to previous work.[8] First, mPEG-SH (1 mM) was added to the nanoparticles overnight to achieve about 1000 ligands on each particle. The PEGylated nanoparticles (1 nM) were then treated with RGD (1 mM) and NLS (1 mM) to achieve 10^4 and 10^5 molar excess, respectively. The number of the ligands bound to the AuNPs was about 25% of the added ligands, evaluated on the basis of Ellman's protocol.[63] The solution was then shaken overnight at room temperature. Excess ligands were removed by centrifugation. A UV−vis spectrometer and zetasizer were used to test the conjugation. Surface modification causes a red shift of the UV−vis spectra due to the change in the dielectric constant of the surrounding environment of AuNSs.

Cell Culture, AuNPs Incubation, and Plasmonic Photothermal Therapy. Human oral squamous cell carcinoma (HSC-3) cells were grown in DMEM medium containing 10% (v/v) FBS and 1% (v/v) antibiotic solution. Cells were kept at 37 °C in a humidified incubator under 5% CO_2. HSC-3 cells were incubated overnight with 2.5 nM AuNRs in complete media and then were exposed to a CW laser (808 nm 5.8 W/cm^2) for different times. The concentration of nanoparticles was carefully chosen to avoid cytotoxicity or perturbation of the cell cycle.

***In Vitro* SERS Measurement.** Time-dependent SERS spectra were collected throughout the NIR laser exposure period to monitor molecular changes in the plasmonic nanoparticle microenvironment during photothermal heating of the AuNRs. The Raman laser was directed into a microscope and, after focusing on the sample by a 50×/0.75 N.A. objective, formed a 1−2 μm spot size. Spectra of molecules in the single cell were measured with a 1200 lines/mm grating and collected by a CCD detector in the range of 400−1800 cm^{-1} using a Renishaw InVia Raman spectrometer. Spectrum baseline was removed using R Package Baseline (version 1.2-1). Dark-field images were taken by a Lumenera Infinity2 CCD camera. For SERS studies, the cells were seeded on glass coverslips in complete growth medium for 24 h to achieve a 40% final confluence before SERS study. The cells were then incubated with 0.05 nM PEG/RGD/NLS-functionalized AuNSs in supplemented DMEM cell culture medium for 24 h.[64] Six hours before the SERS examination, the cell media (with AuNSs) were removed, and a 2.5 nM concentration of AuNRs suspended in supplemented medium was added to the cells to perform PPTT.

Apoptosis/Necrosis Assay. HSC-3 cells were cultured in 12-well plates for 24 h and then treated with a 2.5 nM concentration of AuNRs@NLS for 24 h. After AuNRs incubation, PPTT was applied for different time periods. Before the apoptosis/necrosis assay, the cell culture medium was removed, and cells were collected after trypsinization, followed by washing with cold PBS twice. The cells were the dispersed in 493 mL of Annexin V binding buffer, and 5 μL of Annexin V FITC (BioLegend) and 2 μL of PI (BioLegend, 100 μg/mL) were added to the cell suspension and incubated for 15 min at room temperature.[65] The cells were then filtered and subjected to flow cytometry analysis using a BSR LSR II flow cytometer (BD Biosciences). A 488 nm laser was applied for excitation, and FITC was detected in FL-1 using a 525/30 BP filter, while PI was detected in FL-2 using a 575/30 BP filter. Standard compensation using unstained and single-stained cells was done before performing actual experiments. FlowJo software (Tree Star Inc.) was used for analysis of the viable, apoptotic, and necrotic cells from at least 10 000 events.

Sample Preparation for Metabolomics Experiments. Cells were cultured in 60 mm Petri dishes. The culture media was removed, and cells were washed three times with PBS, followed by a wash with DI water for 2 s and immediate removal of the wash solution. Immediately, 7 mL of metabolite extraction solvents (HPLC-grade methanol:acetonitrile (ACN):0.5 M formic acid (FA), 2:2:1 v/v/v, −20 °C) was added for quenching and lysing the cells.[65] Cells were then scraped down, and the cell suspension was transferred to centrifuge tubes, followed by vortexing and sonication in an ice−water bath and incubation on ice for 15 min for metabolite extraction. The cell suspension was then centrifuged at 20400g at 4 °C for 15 min. Solvent in the sample was evaporated using a CentriVap vacuum concentrator until dryness. The dried samples were kept at −80 °C until analysis.[65]

Sample Preparation for Proteomics Experiments. Cells were cultured in 60 mm Petri dishes. Ice-cold lysis buffer (50 mM HEPES, pH 7.8, 150 mM NaCl, 0.1% SDS (optional), 0.5% SDC, 1% Triton X 100 or NP-40, phosphatase inhibitors) was added directly to the cells after they were washed twice with PBS. The cells were then scraped down and the obtained mixtures homogenized with sonication and vortexing. Cell debris was then removed by centrifugation at 18000g for 20 min at 4 °C. Four volumes of ice-cold acetone:ethanol:acetic acid (50:50:0.1 v/v/v) was added to the supernatant to precipitate the proteins at −20 °C overnight. After centrifugation, the protein pellet was redissolved in denaturing buffer (pH 8.0) containing 8 M urea and 50 mM HEPES, and the protein concentration was tested using a Bradford assay. The disulfide bonds in the protein solution were reduced by 2 mM dithiothreitol at 37 °C for 2 h and subsequently alkylated by addition of 6 mM iodoacetamide. The solution was kept in darkness at room temperature for 40 min.[66]

DOI: 10.1021/jacs.6b08787
J. Am. Chem. Soc. 2016, 138, 15434−15442

Ultra-Performance Liquid Chromatography (UPLC)-MS Metabolomics Analysis. Before analysis, ultra-pure water was added to each dried sample to obtain a final biomass concentration of ~50 000 cells/μL. Samples were further vortexed and then centrifuged at 15 000 rpm for 10 min at 4 °C. The supernatant of each biological sample was transferred to auto-sampler vials for UPLC-MS analysis. Gradient elution was employed in the chromatographic separation method using 0.1% acetic acid in water (mobile phase A) and ACN (mobile phase B), with the following program: 0−1 min, 98% A, 1−3 min 98%−70% A, 3−8 min 70%−50% A, 8−10 min 50%−5% A, 10−15 min 5% A. The flow rate was constant at 0.3 mL min^{-1}. After each sample run, the column was re-equilibrated to the initial conditions in 6 min. The injection volume was 5 μL. The column and auto-sampler tray temperatures were set at 35 and 5 °C, respectively. The mass spectrometer was operated in negative ion mode with a probe capillary voltage of 2.2 kV and a sampling cone voltage of 45.0 V. The source and desolvation gas temperatures were set to 120 and 350 °C, respectively. The nitrogen gas desolvation flow rate was 650 L h^{-1}. The mass spectrometer was calibrated across the range of m/z 50−1200 using a 0.5 mM sodium formate solution prepared in 2-propanol:water (90:10 v/v). Data were drift-corrected during acquisition using a leucine enkephalin (m/z 554.2615) reference spray (Lock Spray) infused at 3 μL min^{-1}. Data were acquired in the range of m/z 50−1200, and the scan time was set to 1 s. Technical duplicates were acquired in all cases. Tandem MS experiments were carried out by fast data-dependent acquisition (fast DDA) or MS/MS in negative polarity and resolution mode. Targeted ions for MS/MS were entered in an include list. A 0.2 s continuum MS survey scan was collected from 50 to 650 Da until the intensity of an individual precursor ion rose above 5000, and then we switched to MS/MS acquisition, in which a 0.1s continuum scan was collected from 30 to 650 Da. The MS/MS scan switched off once the accumulated total ion current reached 100 000 or after 0.25 s. A collision energy profile of 15, 25, and 35 V was applied to the trap cell for ion fragmentation. For the MS/MS method, the scan time was 1 s, and collision voltages between 8 and 30 V were applied to the trap cell. Data acquisition and processing were performed with Masslynx v4.1 software.

LC-MS/MS Analysis for Proteomic Experiments. Purified and dried peptide samples were dissolved in a 10 μL solution containing 5% ACN and 4% FA, and 3 μL was loaded onto a microcapillary column packed with C18 beads (Magic C18AQ, 3 μm, 200 Å, 100 μm × 16 cm, Michrom Bioresources) by a Dionex WPS-3000T PLUS auto-sampler (UltiMate 3000 thermostated Rapid Separation Pulled Loop Well Plate Sampler). Peptides were separated by reverse-phase chromatography using an UltraMate 3000 binary pump with a 110 min gradient of 8−38% ACN (with 0.125% FA) for the triplicates. Peptides were detected with a data-dependent Top 20 method (the 20 most abundant ions were selected for MS2)[67] in a hybrid dual-cell quadrupole linear ion trap−Orbitrap mass spectrometer (LTQ Orbitrap Elite, Thermo Fisher, with Xcalibur 3.0.63 software). For each cycle, each full MS scan (resolution: 60 000) in the Orbitrap at 10^6 AGC target was followed by up to 20 MS/MS for the most intense ions in the LTQ. The selected ions were excluded from further analysis for 90 s. Ions with singly or unassigned charge were not sequenced. For each full MS scan, the maximum ion accumulation time was 1000 ms, and that for MS/MS scans was 50 ms. Mass spectra Raw files were converted into mzXML format and then searched using the SEQUEST algorithm (version 28).[68] Spectra were matched against a database containing sequences of all proteins in the UniProt Human (*Homo sapiens*) database (downloaded in February 2014). The search was performed using following parameters: fully digested with trypsin; up to 3 missed cleavages; fixed modifcations: carbamidomethylation of cysteine (+57.0214); variable modifcations: oxidation of methionine (+15.9949). False discovery rates (FDRs) of peptide and protein identifications were controlled by the target-decoy method.[69,70] Linear discriminant analysis was used to control the quality of peptide identifications using parameters such as Xcorr, precursor mass error, and charge state.[71,72] Peptides less than seven amino acid residues in length were deleted. Furthermore, peptide spectral matches were filtered to <1% FDR.

Data Analysis. For metabolomics, spectral features (t_R, m/z pairs) were extracted from UPLC-MS data using Progenesis QI version 2.0 (Nonlinear Dynamics, Waters Corp.). The data preprocessing procedures included retention time alignment, peak picking, integration, and deconvolution to group the adducts derived from the same compound.

Raw data from metabolomics were normalized using supervised normalization of the microarray (SNM).[73] In the SNM procedure, variances due to biological and technical replicates were adjusted by setting them as variables in the model. A variance explained by different experimental treatments (control, AuNRs@NLS, and AuNRs@NLS/PPTT) was fitted as a biological variable in the model. Clustering analysis on the similarity matrix of metabolomics data was carried out to verify the reproducibility of metabolomics experiments. Hierarchical clustering was done with JMP software (version 9, SAS Institute Inc., Cary, NC). Metabolomics data were log2 transformed before analysis of variance (ANOVA), which was used to detect differential levels of metabolites between control and treatment groups. We fitted models with treatment conditions as fixed effects. A Benjamini−Hochberg 5% FDR correction was used to select differential metabolites.[74] For identified differential metabolites perturbed by PPTT, we used the Mummichog program for network-level metabolites annotation.[75] The MS mode considered in Mummichog was negative ion in order to compute isotopic and adduct species. The metabolites identified as being affected by PPTT were subjected to pathway analysis using the MetaCore pathway analysis software (from Thomson Reuters).

For proteomics, raw data were also normalized using SNM. Clustering analysis on the similarity matrix of data was also carried out to show the reproducibility of the experiments. Hierarchical clustering was done with JMP software. The identified proteins were subjected to pathway analysis using the MetaCore software to study the effect of PPTT.

■ ASSOCIATED CONTENT

Supporting Information

The Supporting Information is available free of charge on the ACS Publications website at DOI: 10.1021/jacs.6b08787.

Cellular uptake of AuNRs using DIC images, cellular toxicity of AuNRs and efficacy of PPTT using cell viability (XTT) assay and apoptosis/necrosis assay, detailed characterization for AuNSs, control experiments and replicated experiments of SERS, clustering and differential analyses of proteomics and metabolomics, quantification accuracy measurement for proteomics, heatmap of phenylalanine derivatives, pathway map of proteomics result, other significant pathways, including Figures S1−S14 and Tables S1 and S2 (PDF)

■ AUTHOR INFORMATION

Corresponding Authors

*melsayed@gatech.edu
*ronghu.wu@chemistry.gatech.edu
*facundo.fernandez@chemistry.gatech.edu

ORCID

Facundo M. Fernández: 0000-0002-0302-2534

Author Contributions

‡M.R.K.A. and Y.W. contributed equally.

Notes

The authors declare no competing financial interest.

DOI: 10.1021/jacs.6b08787
J. Am. Chem. Soc. 2016, 138, 15434−15442

■ ACKNOWLEDGMENTS

We give our special acknowledgement to Dr. Hala R. Ali for help testing the toxicity of the AuNRs using apoptosis/necrosis assay and cell viability assay. We thank Zhenyu Zhou for the help in proteomics experiment. We thank Dr. Kuangcai Chen and Prof. Ning Fang in Gerogia State University for helping in DIC images. We also thank the El-Sayed Undergraduate Research group, including Tsion Assaye, Savita Chapman, Cecily Ritch, Sarah Ghalayini, and Sreenath Raparti, for their critical proofreading of the manuscript. We acknowledge the NSF Division of Chemistry (CHE) Grant 1306269 for funding support.

■ REFERENCES

(1) Qian, X. M.; Peng, X. H.; Ansari, D. O.; Yin-Goen, Q.; Chen, G. Z.; Shin, D. M.; Yang, L.; Young, A. N.; Wang, M. D.; Nie, S. M. *Nat. Biotechnol.* **2008**, *26*, 83.
(2) Kneipp, J.; Kneipp, H.; Kneipp, K. *Chem. Soc. Rev.* **2008**, *37*, 1052.
(3) Ma, C. X.; Harris, J. M. *Appl. Spectrosc.* **2013**, *67*, 801.
(4) Austin, L. A.; Kang, B.; El-Sayed, M. A. *Nano Today* **2015**, *10*, 542.
(5) Jain, P. K.; Huang, X. H.; El-Sayed, I. H.; El-Sayed, M. A. *Acc. Chem. Res.* **2008**, *41*, 1578.
(6) Willets, K. A.; Van Duyne, R. P. *Annu. Rev. Phys. Chem.* **2007**, *58*, 267.
(7) Stiles, P. L.; Dieringer, J. A.; Shah, N. C.; Van Duyne, R. R. *Annu. Rev. Anal. Chem.* **2008**, *1*, 601.
(8) Kang, B.; Austin, L. A.; El-Sayed, M. A. *ACS Nano* **2014**, *8*, 4883.
(9) Keskin, S.; Efeoglu, E.; Kececi, K.; Culha, M. *J. Biomed. Opt.* **2013**, *18*, 037007.
(10) Huang, X. H.; Jain, P. K.; El-Sayed, I. H.; El-Sayed, M. A. *Lasers Med. Sci.* **2008**, *23*, 217.
(11) Alkilany, A. M.; Thompson, L. B.; Boulos, S. P.; Sisco, P. N.; Murphy, C. J. *Adv. Drug Delivery Rev.* **2012**, *64*, 190.
(12) Huang, X. H.; El-Sayed, I. H.; Qian, W.; El-Sayed, M. A. *J. Am. Chem. Soc.* **2006**, *128*, 2115.
(13) Li, Z. M.; Huang, P.; Zhang, X. J.; Lin, J.; Yang, S.; Liu, B.; Gao, F.; Xi, P.; Ren, Q. S.; Cui, D. X. *Mol. Pharmaceutics* **2010**, *7*, 94.
(14) Niidome, T.; Akiyama, Y.; Yamagata, M.; Kawano, T.; Mori, T.; Niidome, Y.; Katayama, Y. *J. Biomater. Sci., Polym. Ed.* **2009**, *20*, 1203.
(15) Peng, X. H.; Macke, M. A.; Shin, H. J. C.; Nannapaneni, S.; Chen, N.; Kim, S.; Chen, Z.; El-Sayed, M. A.; Shin, D. *Cancer Res.* **2015**, *75*, 2451.
(16) Dickerson, E. B.; Dreaden, E. C.; Huang, X.; El-Sayed, I. H.; Chu, H.; Pushpanketh, S.; McDonald, J. F.; El-Sayed, M. A. *Cancer Lett.* **2008**, *269*, 57.
(17) Mukherjee, P.; El-Abbadi, M. M.; Kasperzyk, J. L.; Ranes, M. K.; Seyfried, T. N. *Br. J. Cancer* **2002**, *86*, 1615.
(18) Melamed, J. R.; Edelstein, R. S.; Day, E. S. *ACS Nano* **2015**, *9*, 6.
(19) Perez-Hernandez, M.; del Pino, P.; Mitchell, S. G.; Moros, M.; Stepien, G.; Pelaz, B.; Parak, W. J.; Galvez, E. M.; Pardo, J.; de la Fuente, J. M. *ACS Nano* **2015**, *9*, 52.
(20) Narayanan, N.; Nair, L. V.; Karunakaran, V.; Joseph, M. M.; Nair, J. B.; Ramya, A. N.; Jayasree, R. S.; Maiti, K. K. *Nanoscale* **2016**, *8*, 11392.
(21) Aliaga, A. E.; Osorio-Roman, I.; Leyton, P.; Garrido, C.; Carcamo, J.; Caniulef, C.; Celis, F.; Diaz, G.; Clavijo, E.; Gomez-Jeria, J. S.; Campos-Vallette, M. M. *J. Raman Spectrosc.* **2009**, *40*, 164.
(22) Zhu, G. Y.; Zhu, X.; Fan, Q.; Wan, X. L. *Spectrochim. Acta, Part A* **2011**, *78*, 1187.
(23) Maiti, N. C.; Apetri, M. M.; Zagorski, M. G.; Carey, P. R.; Anderson, V. E. *J. Am. Chem. Soc.* **2004**, *126*, 2399.
(24) Ali, M. R. K.; Snyder, B.; El-Sayed, M. A. *Langmuir* **2012**, *28*, 9807.
(25) Mackey, M. A.; Ali, M. R. K.; Austin, L. A.; Near, R. D.; El-Sayed, M. A. *J. Phys. Chem. B* **2014**, *118*, 1319.
(26) Prencipe, G.; Tabakman, S. M.; Welsher, K.; Liu, Z.; Goodwin, A. P.; Zhang, L.; Henry, J.; Dai, H. *J. Am. Chem. Soc.* **2009**, *131*, 4783.
(27) Ruoslahti, E.; Pierschbacher, M. D. *Cell* **1986**, *44*, 517.
(28) Kalderon, D.; Roberts, B. L.; Richardson, W. D.; Smith, A. E. *Cell* **1984**, *39*, 499.
(29) Ali, M. R. K.; Panikkanvalappil, S. R.; El-Sayed, M. A. *J. Am. Chem. Soc.* **2014**, *136*, 4464.
(30) Ali, M. R. K.; Ali, H. R.; Rankin, C. R.; El-Sayed, M. A. *Biomaterials* **2016**, *102*, 1.
(31) Panikkanvalappil, S. R.; Mackey, M. A.; El-Sayed, M. A. *J. Am. Chem. Soc.* **2013**, *135*, 4815.
(32) Panikkanvalappil, S. R.; Hira, S. M.; Mahmoud, M. A.; El-Sayed, M. A. *J. Am. Chem. Soc.* **2014**, *136*, 15961.
(33) Kang, B.; Austin, L. A.; El-Sayed, M. A. *Nano Lett.* **2012**, *12*, 5369.
(34) Fodor, S. P. A.; Copeland, R. A.; Grygon, C. A.; Spiro, T. G. *J. Am. Chem. Soc.* **1989**, *111*, 5509.
(35) Hernandez, B.; Pfluger, F.; Kruglik, S. G.; Ghomi, M. *J. Raman Spectrosc.* **2013**, *44*, 827.
(36) Zhang, J. J.; Huang, Q.; Yao, G. H.; Ke, Z. G.; Zhang, H.; Lu, Y. L. *J. Mol. Struct.* **2014**, *1072*, 195.
(37) Kim, S. K.; Kim, M. S.; Suh, S. W. *J. Raman Spectrosc.* **1987**, *18*, 171.
(38) Okada, M.; Smith, N. I.; Palonpon, A. F.; Endo, H.; Kawata, S.; Sodeoka, M.; Fujita, K. *Proc. Natl. Acad. Sci. U. S. A.* **2012**, *109*, 28.
(39) Hamada, K.; Fujita, K.; Smith, N. I.; Kobayashi, M.; Inouye, Y.; Kawata, S. *J. Biomed. Opt.* **2008**, *13*, 044027.
(40) Zhang, Y.; Gu, X.; Yuan, X. *Eur. J. Neurosci.* **2007**, *25*, 1341.
(41) Huang, X.; Lu, Z.; Lv, Z.; Yu, T.; Yang, P.; Shen, Y.; Ding, Y.; Fu, D.; Zhang, X.; Fu, Q.; Yu, Y. *PLoS One* **2013**, *8*, e71553.
(42) Lo, Y. W.; Lin, S. T.; Chang, S. J.; Chan, C. H.; Lyu, K. W.; Chang, J. F.; May, E. W.; Lin, D. Y.; Chou, H. C.; Chan, H. L. *J. Cell. Mol. Med.* **2015**, *19*, 744.
(43) Gonzalez, V. M.; Fuertes, M. A.; Alonso, C.; Perez, J. M. *Mol. Pharmacol.* **2001**, *59*, 657.
(44) Kageyama, T.; Nagashio, R.; Ryuge, S.; Matsumoto, T.; Iyoda, A.; Satoh, Y.; Masuda, N.; Jiang, S. X.; Saegusa, M.; Sato, Y. *Asian Pac. J. Cancer Prev.* **2011**, *12*, 3457.
(45) Sato, A.; Hiramoto, A.; Satake, A.; Miyazaki, E.; Naito, T.; Wataya, Y.; Kim, H. S. *Nucleosides, Nucleotides Nucleic Acids* **2008**, *27*, 433.
(46) Freund, A.; Laberge, R. M.; Demaria, M.; Campisi. *J. Mol. Biol. Cell* **2012**, *23*, 2066.
(47) Rao, L.; Perez, D.; White, E. *J. Cell Biol.* **1996**, *135*, 1441.
(48) Zha, J.; Harada, H.; Yang, E.; Jockel, J.; Korsmeyer, S. J. *Cell* **1996**, *87*, 619.
(49) Schurmann, A.; Mooney, A. F.; Sanders, L. C.; Sells, M. A.; Wang, H. G.; Reed, J. C.; Bokoch, G. M. *Mol. Cell. Biol.* **2000**, *20*, 453.
(50) Jin, S.; Zhuo, Y.; Guo, W.; Field, J. *J. Biol. Chem.* **2005**, *280*, 24698.
(51) Koyanagi, M.; Takahashi, J.; Arakawa, Y.; Doi, D.; Fukuda, H.; Hayashi, H.; Narumiya, S.; Hashimoto, N. *J. Neurosci. Res.* **2008**, *86*, 270.
(52) Iwasaki, T.; Katayama, T.; Kohama, K.; Endo, Y.; Sawasaki, T. *Mol. Biol. Cell* **2013**, *24*, 748.
(53) Fehrenbacher, N.; Bastholm, L.; Kirkegaard-Sorensen, T.; Rafn, B.; Bottzauw, T.; Nielsen, C.; Weber, E.; Shirasawa, S.; Kallunki, T.; Jaattela, M. *Cancer Res.* **2008**, *68*, 6623.
(54) Kaufman, S. *Adv. Enzymol. Relat. Areas Mol. Biol.* **1993**, *67*, 77.
(55) Martinez, A.; Knappskog, P. M.; Olafsdottir, S.; Doskeland, A. P.; Eiken, H. G.; Svebak, R. M.; Bozzini, M.; Apold, J.; Flatmark, T. *Biochem. J.* **1995**, *306*, 589.
(56) Moller, N.; Meek, S.; Bigelow, M.; Andrews, J.; Nair, K. S. *Proc. Natl. Acad. Sci. U. S. A.* **2000**, *97*, 1242.
(57) Kang, B.; Mackey, M. A.; El-Sayed, M. A. *J. Am. Chem. Soc.* **2010**, *132*, 1517.
(58) Pan, Y.; Neuss, S.; Leifert, A.; Fischler, M.; Wen, F.; Simon, U.; Schmid, G.; Brandau, W.; Jahnen-Dechent, W. *Small* **2007**, *3*, 1941.
(59) Seyfried, T. N.; Mukherjee, P. *Nutr. Metab.* **2005**, *2*, 30.

DOI: 10.1021/jacs.6b08787
J. Am. Chem. Soc. 2016, 138, 15434−15442

(60) Mukherjee, P.; Abate, L. E.; Seyfried, T. N. *Clin. Cancer Res.* **2004**, *10*, 5622.
(61) Mukherjee, P.; El-Abbadi, M. M.; Kasperzyk, J. L.; Ranes, M. K.; Seyfried, T. N. *Br. J. Cancer* **2002**, *86*, 1615.
(62) Turkevich, J.; Stevenson, P. C.; Hillier, J. *Discuss. Faraday Soc.* **1951**, *11*, 55.
(63) Ellman, G. L. *Arch. Biochem. Biophys.* **1959**, *82*, 70.
(64) Austin, L. A.; Ahmad, S.; Kang, B.; Rommel, K. R.; Mahmoud, M.; Peek, M. E.; El-Sayed, M. A. *Toxicol. In Vitro* **2015**, *29*, 694.
(65) Martano, G.; Delmotte, N.; Kiefer, P.; Christen, P.; Kentner, D.; Bumann, D.; Vorholt, J. A. *Nat. Protoc.* **2015**, *10*, 1.
(66) Wu, Y.; Wang, F. J.; Liu, Z. Y.; Qin, H. Q.; Song, C. X.; Huang, J. F.; Bian, Y. Y.; Wei, X. L.; Dong, J.; Zou, H. F. *Chem. Commun.* **2014**, *50*, 1708.
(67) Xiao, H.; Tang, G. X.; Wu, R. *Anal. Chem.* **2016**, *88*, 3324.
(68) Eng, J. K.; McCormack, A. L.; Yates, J. R. *J. Am. Soc. Mass Spectrom.* **1994**, *5*, 976.
(69) Elias, J. E.; Gygi, S. P. *Nat. Methods* **2007**, *4*, 207.
(70) Peng, J.; Elias, J. E.; Thoreen, C. C.; Licklider, L. J.; Gygi, S. P. *J. Proteome Res.* **2003**, *2*, 43.
(71) Kall, L.; Canterbury, J. D.; Weston, J.; Noble, W. S.; MacCoss, M. J. *Nat. Methods* **2007**, *4*, 923.
(72) Huttlin, E. L.; Jedrychowski, M. P.; Elias, J. E.; Goswami, T.; Rad, R.; Beausoleil, S. A.; Villen, J.; Haas, W.; Sowa, M. E.; Gygi, S. P. *Cell* **2010**, *143*, 1174.
(73) Mecham, B. H.; Nelson, P. S.; Storey, J. D. *Bioinformatics* **2010**, *26*, 1308.
(74) Benjamini, Y.; Hochberg, Y. *J. R. Stat. Soc. B-Methodol.* **1995**, *57*, 289.
(75) Li, S. Z.; Park, Y.; Duraisingham, S.; Strobel, F. H.; Khan, N.; Soltow, Q. A.; Jones, D. P.; Pulendran, B. *PLoS Comput. Biol.* **2013**, *9*, e1003123.

DOI: 10.1021/jacs.6b08787
J. Am. Chem. Soc. 2016, 138, 15434−15442